Electronic Supplementary Information

Untangling the Intertwined: Metallic to Semiconducting Phase Transition of Colloidal MoS_2 Nanoplatelets and Nanosheets

André Niebur,[†a,b] Aljoscha Söll,[†a] Philipp Haizmann,[c] Onno Strolka,[a,b,c] Dominik Rudolph,[a,b] Kevin Tran,[d,e] Franz Renz,[d,e] André Philipp Frauendorf,[f] Jens Hübner,[e,f] Heiko Peisert,[c] Marcus Scheele[c] and Jannika Lauth*[a,b,c,e]

---

[a] *Institute of Physical Chemistry and Electrochemistry, Leibniz University Hannover, Callinstr. 3a, D-30167 Hannover, Germany*
[b] *Cluster of Excellence PhoenixD (Photonics, Optics, and Engineering – Innovation Across Disciplines), Hannover, Germany*
[c] *Institute of Physical and Theoretical Chemistry, University of Tübingen, Auf der Morgenstelle 18, D-72076 Tübingen, Germany*
[d] *Institute of Inorganic Chemistry, Leibniz University Hannover, Callinstr. 9, D-30167 Hannover, Germany*
[e] *Laboratory of Nano and Quantum Engineering (LNQE), Leibniz University Hannover, Schneiderberg 39, D-30167 Hannover, Germany*
[f] *Institute of Solid State Physics, Leibniz University Hannover, Appelstr. 2, D-30167 Hannover, Germany*
[†] *Equal contribution.*
* jannika.lauth@uni-tuebingen.de

Stabilization of Colloidal MoS_2 NPLs and NSs by Oleic Acid and Oleylamine

Fourier-Transform Infrared (FTIR) transmission spectra of MoS_2 NPLs and NSs were obtained using a Tensor 27 spectrometer from Bruker. Washed samples were added to KBr and were subsequently dried at 110 °C for 24 h. Discs were pressed out of the KBr/MoS_2 mixture. FTIR spectra of OA, OlAm and an OA:OlAm (1:10) mixture were measured using a Cary 630 FTIR spectrometer by Agilent Technologies, utilizing Attenuated Total Reflection (ATR).

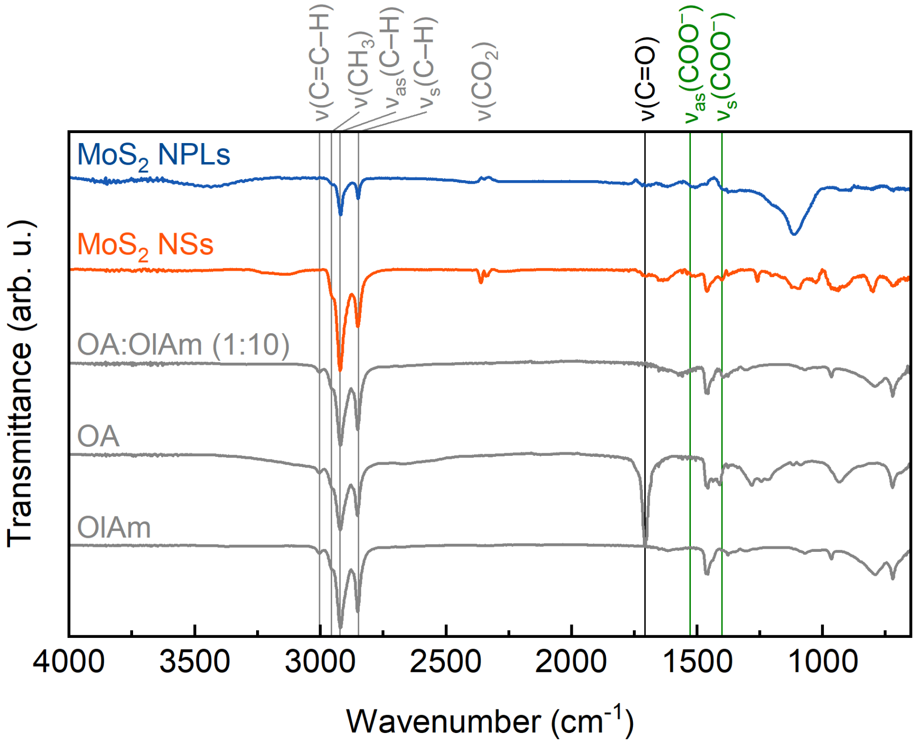

Figure S1. FTIR spectra of MoS_2 NPLs and NSs, pure oleic acid, oleylamine and a 1:10-mixture of oleic acid and oleylamine used to dissolve the Mo precursor. s = symmetric, as = antisymmetric.

The vibration modes between 2800 cm^{-1} and 3050 cm^{-1} present in all samples are caused by the oleyl group in OA or OlAm. In detail, the modes are attributed to the C=C–H stretching (3004 cm^{-1})[1], the antisymmetric stretching of CH_3 (2958 cm^{-1})[2], and the antisymmetric and symmetric stretching of non-terminal C–H (2922 cm^{-1} and 2850 cm^{-1})[1]. These signals suggest that OA or OlAm is present in the washed samples. In pure oleic acid C=O stretching appears at 1708 cm^{-1} (black line) and is replaced by two modes of the COO^- group at 1402 cm^{-1} and 1530 cm^{-1} if the OA is present as oleate (green lines)[1,3]. Both samples, MoS_2 NPLs and NSs, show a low intensity C=O stretching signal, suggesting that OA acts as a monodentate ligand. The characteristic symmetric and antisymmetric COO^- stretch modes at 1402 cm^{-1} and 1530 cm^{-1} are not clearly visible in the samples.

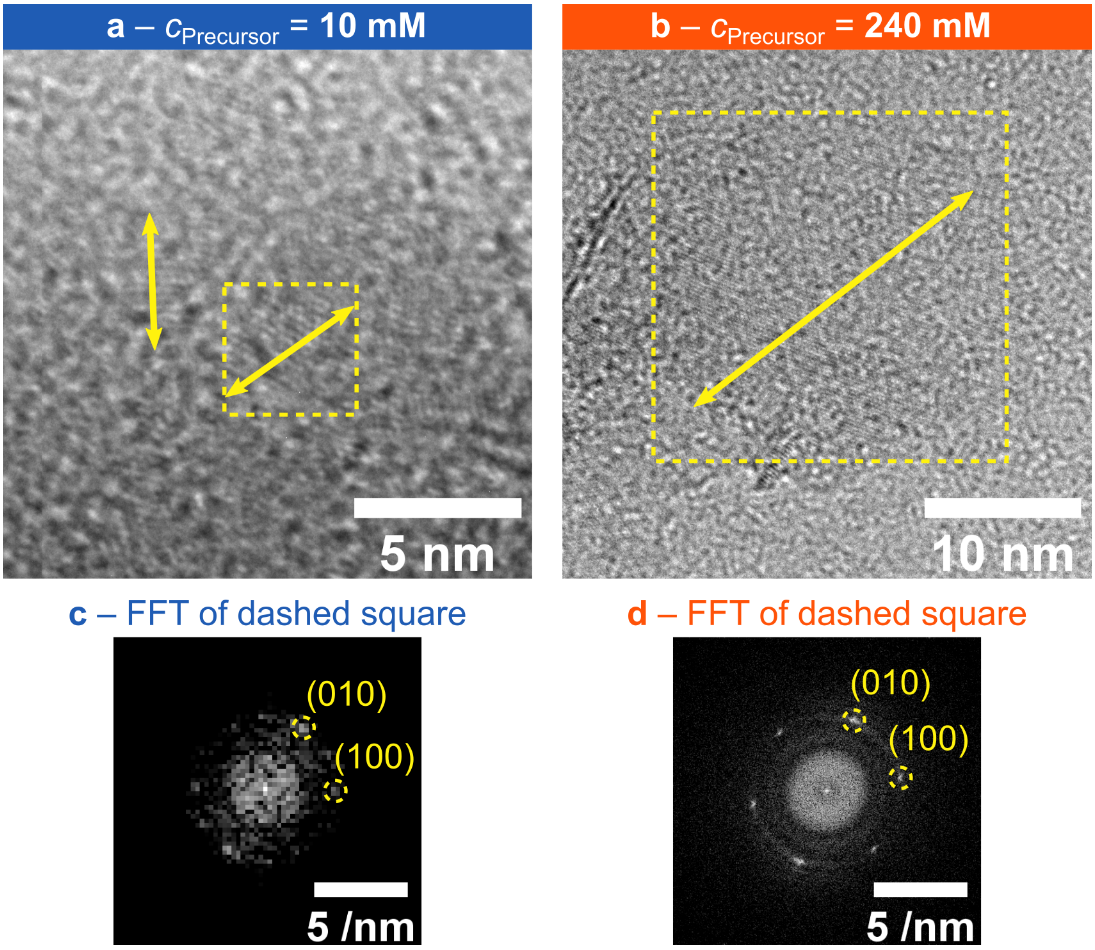

Figure S2. HRTEM images of flat-on oriented 2D MoS_2 NPLs and NSs synthesized with Mo-precursor concentrations of (**a**) 10 mM and (**b**) 240 mM. NPL and NS sizes are identified by a difference in contrast to the background and by domains of lattice planes (indicated by yellow arrows). (**c**) and (**d**) are FFT of the area in dashed squares in (**a**) and (**b**), respectively. Both images show the hexagonal pattern of the 2*H* MoS_2 crystal phase for NPLs and NSs.

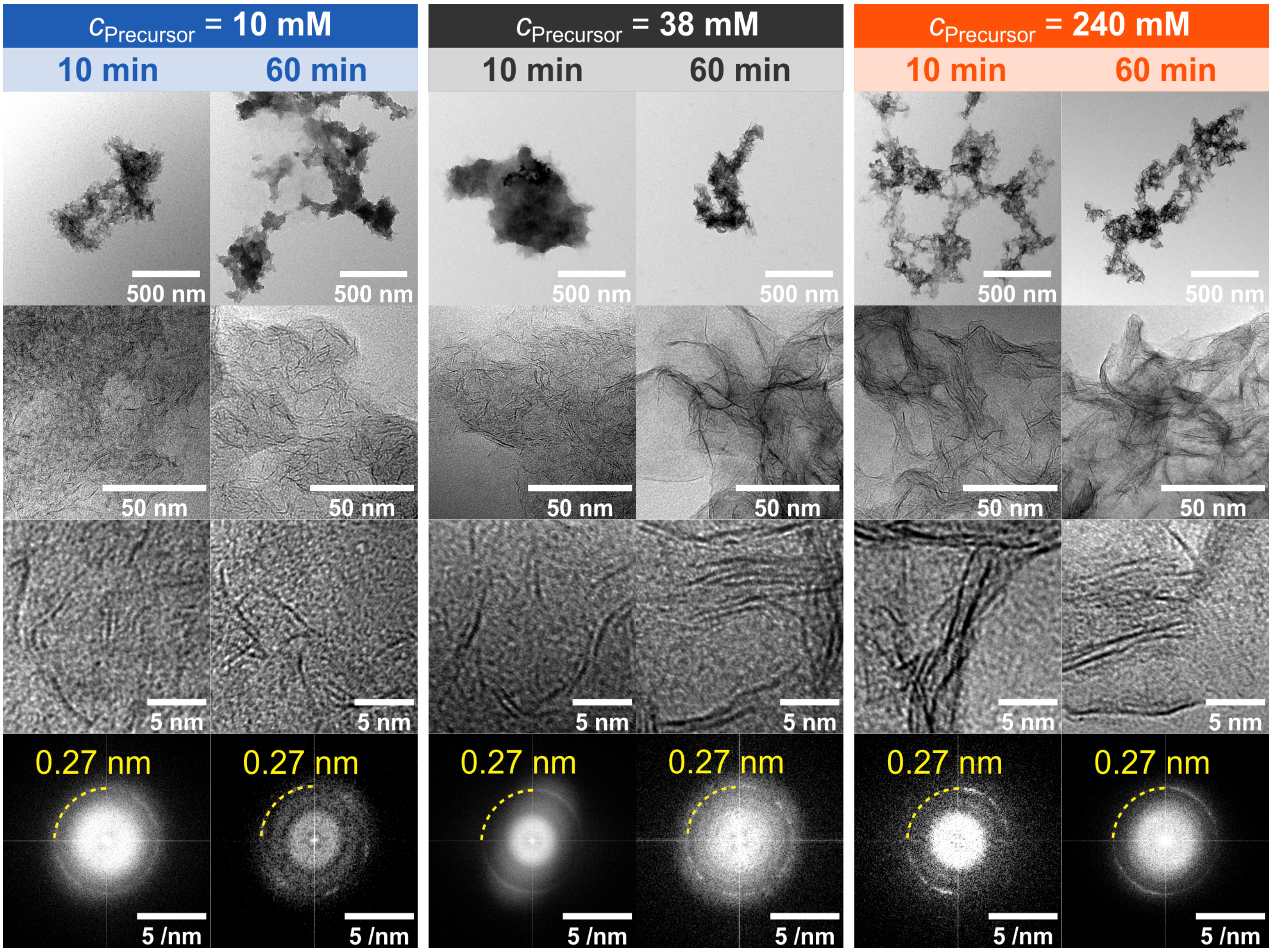

Figure S3. TEM and HRTEM images of MoS_2 NPLs and NSs synthesized by using different precursor concentrations: 10 mM (blue), 38 mM (grey), and 240 mM (orange). For each precursor concentration TEM images are shown after 10 min and 60 min of reaction time. The last row shows a Fourier-transformed HRTEM image exhibiting the same lattice constant of 0.27 nm for all MoS_2 samples.

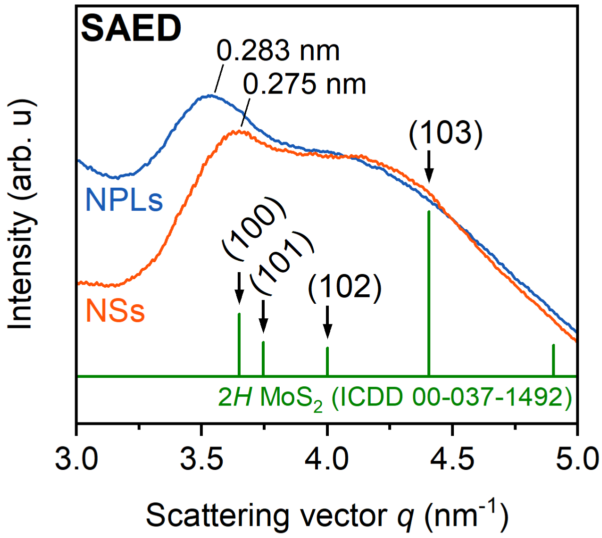

Figure S4. SAED measurements of single MoS_2 NPLs and NSs shown in Figure 2a and 2b. Both samples show the typical (100) reflex overlapped by a broad (103) reflex. The (100) reflex of the MoS_2 NSs matches the literature value of 0.274 nm for bulk 2*H* MoS_2 (ICDD 00-037-1492). For NPLs the (100) reflex is shifted to 0.283 nm corresponding to a lattice expansion of 3%.

Powder X-ray diffraction (PXRD).

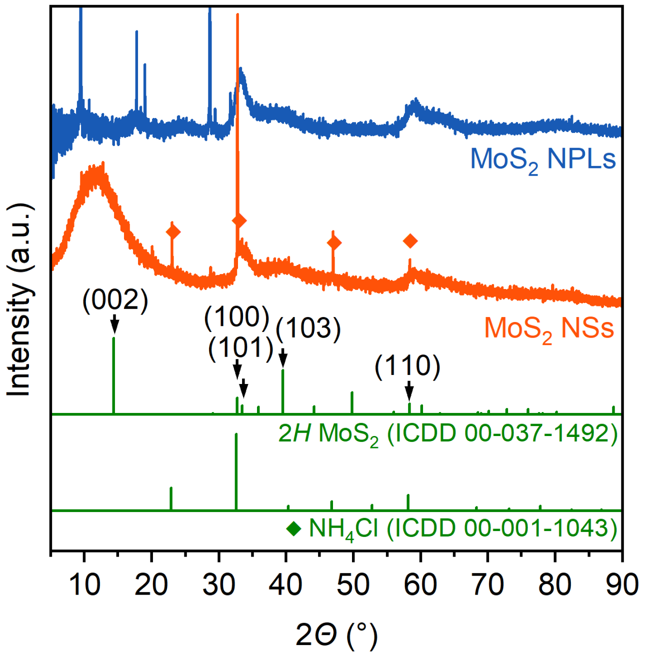

Figure S5. XRD patterns are associated with the 2*H* crystal phase of MoS$_2$. The dominant reflexes are the (002), (100), (101), (103) and (110) lattice planes and are broadened due to the spatial confinement of the NPLs and NSs. Most of the narrow reflexes are attributed to in situ formed impurities such as NH$_4$Cl.

Powder X-ray diffractograms were recorded with a Bruker D8 ADVANCE diffractometer with a Cu Kα1 source (40 kV, 30 mA). Samples were prepared on a silicon single crystal by drop casting.

Figure S3 shows XRD patterns for 10 mM and 240 mM Mo-precursor concentrations respectively with a comparison to bulk MoS$_2$ in the 2*H* crystal phase. The (002) reflex has a special significance for the estimation of the MoS$_2$ layer thickness due to repeating (002) lattice planes which correspond to formation of MoS$_2$ multilayers. Fewer MoS$_2$ layers lead to a broadening of the (002) reflex. MoS$_2$ NSs synthesized by a low 10 mM Mo-precursor concentration lack the (002) reflex, implying the presence of mainly monolayers.[4] In contrast, the XRD pattern of high 240 mM Mo precursor MoS$_2$ NSs exhibit a (002) reflex. This reflex is broadened as is expected for multilayer NS and shifted to 11.72° compared to the bulk reflex at 14.38°. This shift corresponds to an enlarged Mo-to-Mo layer distance of 0.75 nm (0.615 nm in bulk[5,6]) and is caused by the colloidal NSs having a twisted shape and are therefore not optimally stacked. Figure S3 shows that the most prominent reflexes are attributed to the lattice planes (100), (101), (103) and (110) of MoS$_2$ in the 2*H* crystal phase. These reflexes are strongly broadened, which is expected for confined systems and usually observed in TMDC NS diffractograms in the literature.[4,7] Due to the similarity of both crystal phases combined with the strong broadening, a distinction between the 2*H* and the *1T* phase cannot be made with absolute certainty by XRD.

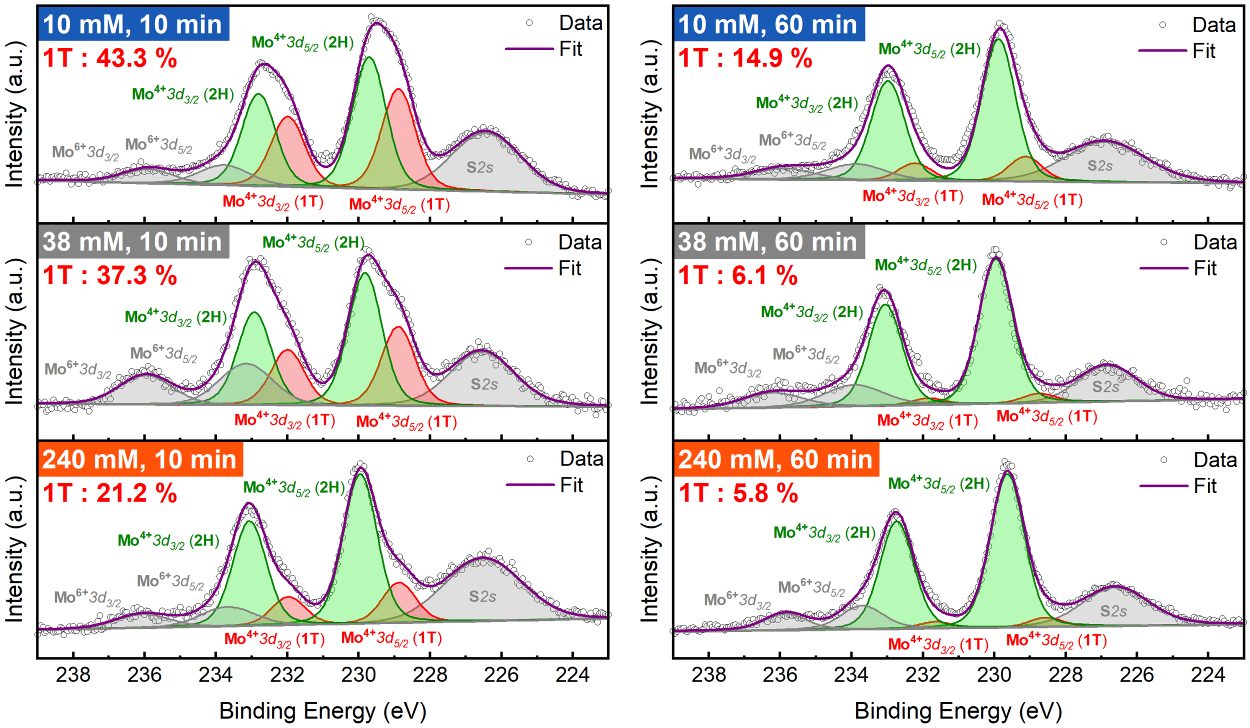

Figure S6 XPS spectra of NPLs and NSs synthesized with different Mo-precursor concentrations. The synthesis parameters (precursor concentration and synthesis time) are indicated in the upper left corner. The fraction of the signal area associated with the 1*T* phase in the total Mo^{4+} signal area is given.

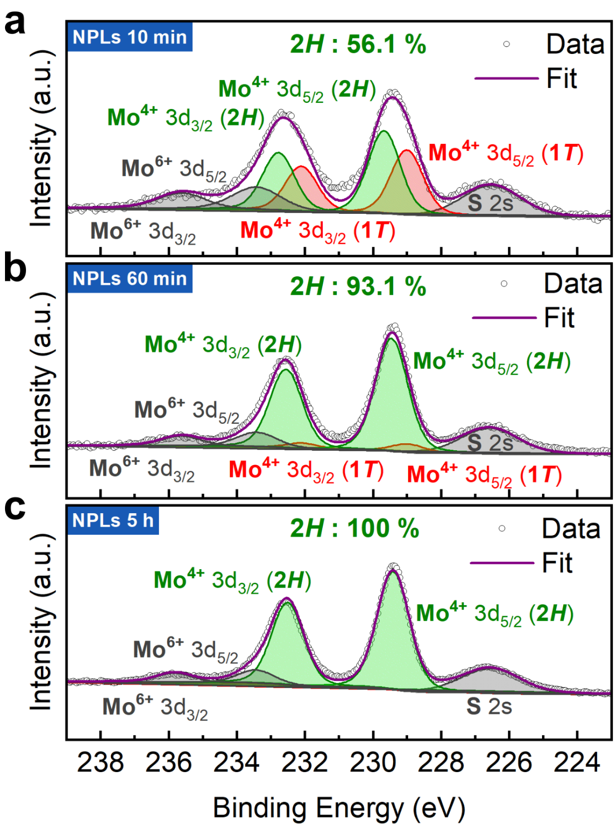

Figure S7 XPS spectra of MoS_2 NPLs synthesized with a 10 mM Mo-precursor concentration for reaction. Aliquots were taken after the injection of 10 min (a), 60 min of reaction (b) and 5 h of reaction at 320 °C (c). After the injection, NPLs are 2*H*/1*T* phase mixed (56:44) and transformed into the semiconducting 2*H* phase during the reaction.

Fitting of the absorption spectroscopy data

Derivative absorbance spectra and transient absorbance spectra were normalized to the B exciton feature between 2 eV and 2.2 eV. The normalized data were fitted with the sum of a constant background and one or two Gaussian curves for MoS_2 NPLs or NSs, respectively.

$$A_{\mathrm{fit}} = A_0 + g_{\mathrm{A}} + g_{\mathrm{B}}$$

$$= A_0 + \sqrt{\frac{2}{\pi}}\left(\frac{Amp_{\mathrm{A}}}{w_{\mathrm{A}}}e^{-2\frac{\left(x-x_{\mathrm{c,A}}\right)^2}{w_{\mathrm{A}}^2}} + \frac{Amp_{\mathrm{B}}}{w_{\mathrm{B}}}e^{-2\frac{\left(x-x_{\mathrm{c,B}}\right)^2}{w_{\mathrm{B}}^2}}\right),$$

with A_0 being a constant offset and – with indices A and B, referring to the respective exciton – g the Gaussian function, Amp the amplitude, w the width, and x_c the energetic center of the Gaussian function. The fitted parameters are Amp, w, and x_c, and subsequently the full width at half maximum ($FWHM$) is calculated by

$$FWHM = \sqrt{2\ln(2)} \cdot w.$$

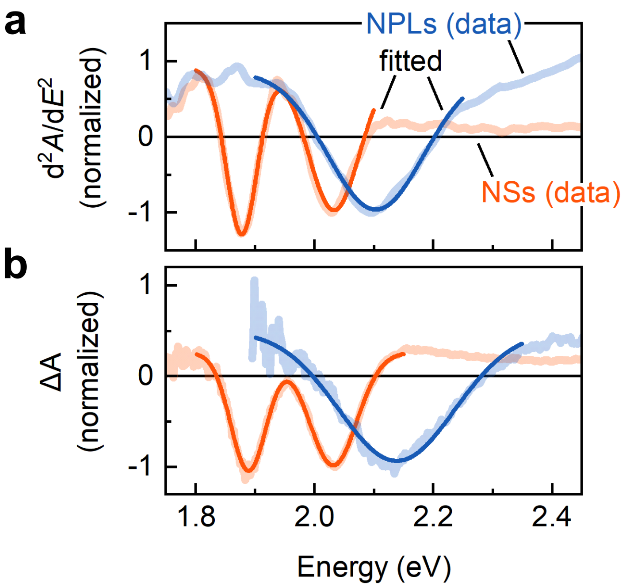

Figure S8. Fitting of **a** – d^2A/dE^2 and **b** – ΔA data: The measured spectra are normalized and fitted with one or two Gaussian functions to get information about the energetic position and FWHM of the respective A and B excitonic feature.

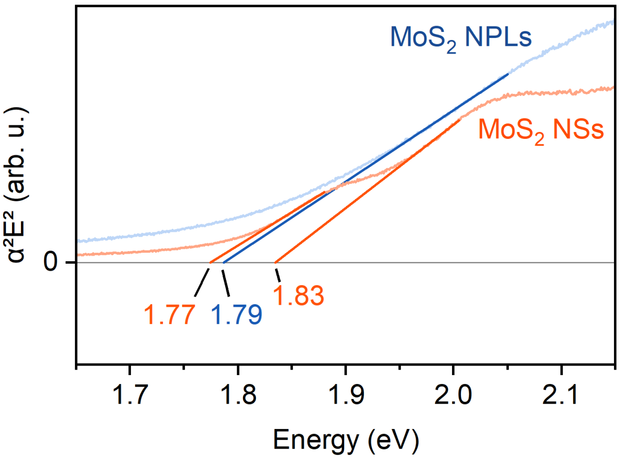

Figure S9. Tauc plot of MoS$_2$ NPLs and NSs (blue and orange, respectively). The lateral size of the sample does not affect the absorption threshold, which is 1.8 eV in both cases. Note, that the determined threshold corresponds to the band gap subtracted by the exciton binding energy and a broadening parameter.

References

(1) Luther, J. M.; Law, M.; Song, Q.; Perkins, C. L.; Beard, M. C.; Nozik, A. J. Structural, Optical, and Electrical Properties of Self-Assembled Films of PbSe Nanocrystals Treated with 1,2-Ethanedithiol. *ACS Nano* **2008**, *2* (2), 271–280. https://doi.org/10.1021/nn7003348.

(2) Dibenedetto, C. N.; Sibillano, T.; Brescia, R.; Prato, M.; Triggiani, L.; Giannini, C.; Panniello, A.; Corricelli, M.; Comparelli, R.; Ingrosso, C.; Depalo, N.; Agostiano, A.; Curri, M. L.; Striccoli, M.; Fanizza, E. PbS Quantum Dots Decorating TiO$_2$ Nanocrystals: Synthesis, Topology, and Optical Properties of the Colloidal Hybrid Architecture. *Molecules* **2020**, *25* (12), 2939. https://doi.org/10.3390/molecules25122939.

(3) Kroupa, D. M.; Vörös, M.; Brawand, N. P.; McNichols, B. W.; Miller, E. M.; Gu, J.; Nozik, A. J.; Sellinger, A.; Galli, G.; Beard, M. C. Tuning Colloidal Quantum Dot Band Edge Positions through Solution-Phase Surface Chemistry Modification. *Nat. Commun.* **2017**, *8* (1), 15257. https://doi.org/10.1038/ncomms15257.

(4) Zhou, M.; Zhang, Z.; Huang, K.; Shi, Z.; Xie, R.; Yang, W. Colloidal Preparation and Electrocatalytic Hydrogen Production of MoS$_2$ and WS$_2$ Nanosheets with Controllable Lateral Sizes and Layer Numbers. *Nanoscale* **2016**, *8* (33), 15262–15272. https://doi.org/10.1039/C6NR04775K.

(5) Wakabayashi, N.; Smith, H. G.; Nicklow, R. M. Lattice Dynamics of Hexagonal MoS$_2$ Studied by Neutron Scattering. *Phys. Rev. B* **1975**, *12* (2), 659–663. https://doi.org/10.1103/PhysRevB.12.659.

(6) Srivastava, S. K.; Avasthi, B. N.; Mathur, B. K. Synthesis and Characterization of Indium Intercalation Compound of MoS$_2$, In$_x$MoS$_2$ ($0 \leq x \leq 1$). *J. Mater. Sci. Lett.* **1984**, *3* (8), 671–673. https://doi.org/10.1007/BF00719919.

(7) Mahler, B.; Hoepfner, V.; Liao, K.; Ozin, G. A. Colloidal Synthesis of 1T-WS$_2$ and 2H-WS$_2$ Nanosheets: Applications for Photocatalytic Hydrogen Evolution. *J. Am. Chem. Soc.* **2014**, *136* (40), 14121–14127. https://doi.org/10.1021/ja506261t.